Nearly arbitrary on-chip optical filters for ultrafast pulse shaping

Ian W. Frank,[1,2] Yinan Zhang,[1,2] and Marko Loncar[1,2]

[1]*Harvard School of Engineering and Applied Science, 29 Oxford St, Cambridge, MA 02138, USA*
[2]*These authors contributed equally to this work*
[*]*loncar@seas.harvard.edu*

Abstract: We demonstrate a reverse design method for realizing a broad range of optical filters based on integrated optical waveguides and experimentally verify example designs on a silicon-on-insulator (SOI) platform. The reflectance-based filters allow for control of both phase and amplitude of the optical response. Among this device's many potential applications we highlight and numerically demonstrate its use for ultrafast on-chip pulse shaping.

OCIS codes: (320.0320) Ultrafast optics; (320.5540) Pulse shaping; (120.2440) Filters; (230.7370) Waveguides.

References and links

1. E. Yablonovitch and T. J. Gmitter, "Photonic band structure: the face-centered-cubic case," Phys. Rev. Lett. **63**(18), 1950–1953 (1989).
2. K. M. Ho, C. T. Chan, and C. M. Soukoulis, "Existence of a Photonic Gap in Periodic Dielectric Structures," Phys. Rev. Lett. **65**(25), 3152–3155 (1990).
3. J. D. Joannopoulos, S. G. Johnson, J. N. Winn, and R. D. Meade, *Photonic Crystals: Molding the Flow of Light*, (Princeton University Press, 2008).
4. J. C. Knight, T. A. Birks, P. S. Russell, and D. M. Atkin, "All-silica single-mode optical fiber with photonic crystal cladding," Opt. Lett. **21**(19), 1547–1549 (1996).
5. K. J. Vahala, "Optical Microcavities," Nature **424**(6950), 839–846 (2003).
6. E. Ozbay, "Plasmonics: Merging Photonics and Electronics at Nanoscale Dimensions," Science **311**(5758), 189–193 (2006).
7. W. L. Barnes, A. Dereux, and T. W. Ebbesen, "Surface plasmon subwavelength optics," Nature **424**(6950), 824–830 (2003).
8. D. R. Smith, J. B. Pendry, and M. C. K. Wiltshire, "Metamaterials and Negative Refractive Index," Science **305**(5685), 788–792 (2004).
9. V. M. Shalaev, "'Optical negative-index metamaterials," Nat. Photonics **1**(1), 41–48 (2007).
10. G. Steinmeyer, "A review of ultrafast optics and optoelectronics," J. Opt. A, Pure Appl. Opt. **5**(1), R1–R5 (2003).
11. C. Brif, R. Chakrabarti, and H. Rabitz, "Control of quantum phenomena: past, present, and future," New J. Phys. **12**(7), 075008 (2010).
12. Y. Zhang, C. Li, and M. Lončar, "Optimal Broadband Antireflective Taper," Opt. Lett. **38**(5), 646–648 (2013).
13. G. B. Arkfen and H. J. Webber, *Mathematical Methods for Physicist*s (Academic Press, 2005).
14. M. Verbist, D. Van Thourhout, and W. Bogaerts, "Weak gratings in silicon-on-insulator for spectral filters based on volume holography," Opt. Lett. **38**(3), 386–388 (2013).
15. T. Vallius, "Tailored bandgaps: iterative algorithms of diffractive optics," Opt. Express **21**(11), 13810–13817 (2013).
16. D. T. H. Tan, K. Ikeda, R. E. Saperstein, B. Slutsky, and Y. Fainman, "Chip-scale dispersion engineering using chirped vertical gratings," Opt. Lett. **33**(24), 3013–3015 (2008).
17. D. T. H. Tan, K. Ikeda, and Y. Fainman, "Coupled chirped vertical gratings for on-chip group velocity dispersion engineering," APL **95**, 141109 (2009).
18. D. T. H. Tan, P. C. Sun, and Y. Fainman, "Monolithic nonlinear pulse compressor on a silicon chip," Nat Commun **1**(8), 116 (2010).
19. A. M. Weiner, "Femtosecond pulse shaping using spatial light modulators," Rev. Sci. Instrum. **71**(5), 1929–1960 (2000).
20. A. Präkelt, M. Wollenhaupt, A. Assion, Ch. Horn, C. Sarpe-Tudoran, M. Winter, and T. Baumert, "Compact, robust, and flexible setup for femtosecond pulse shaping," Rev. Sci. Instrum. **74**(11), 4950–4953 (2003).
21. D. Meshulach and Y. Silberberg, "Coherent quantum control of multiphoton transitions by shaped ultrashort optical pulses," PRA **60**(2), 1287–1292 (1999).
22. P. Nuernberger, G. Vogt, T. Brixner, and G. Gerber, "Femtosecond quantum control of molecular dynamics in the condensed phase," Phys. Chem. Chem. Phys. **9**(20), 2470–2497 (2007).

#214559 - $15.00 USD Received 23 Jun 2014; revised 26 Aug 2014; accepted 26 Aug 2014; published 9 Sep 2014

23. A. Monmayrant, S. Weber, and B. Chatel, "A newcomer's guide to ultrashort pulse shaping and characterization," J. Phys. At. Mol. Opt. Phys. **43**(10), 103001 (2010).

24. Hamming pulse shape: $w(n) = A\left[0.54 - 0.46\cos\left(2\pi\frac{n}{N}\right)\right], 0 \le n \le N$.

1. Introduction

The advent of photonic bandgap materials has led to incredible progress in the ability to confine and guide light [1–3]. However, the previously developed methods have operated either in broad stop and pass bands [4] or with extremely narrow-band – resonance – regimes [5]. Additional fields such as plasmonics [6,7] and metamaterials [8,9], provide methods for designing structures that can manipulate light, but even there, we see limitations on the diversity of spectral response from a single device. A significant advance is the possibility of designing a structure that can reflect spectral features of nearly arbitrary bandwidth, amplitude, and phase. We present a simple and fast method for designing such a structure. While this method can be generally applied to any material system where the refractive index profile can be controlled along one axis, we have concentrated on implementing arbitrary reflective filters in compact, on-chip silicon-on-insulator (SOI) waveguides. These integrated filters have myriad applications from on-chip signal routing to compact, ultra-fast pulse shaping [10]; the latter being of significant interest for high-speed optical communication and quantum control experiments [11].

2. Reverse design method and refinements

In our recent work we have studied a region with a refractive index modulation in one dimension [12] and derived the Fourier transform relationship between the reflectance spectrum and the refractive index profile [n(x)]. This simple relationship is possible because we are able to use the wave impedance (inversely proportional to the refractive index in a plane wave) to simplify the form of Maxwell's equations. The following, derived from 1D Maxwell's equations in time harmonic form, describes the non-linear, ordinary differential equation for the ratio of the amplitudes of the reverse (reflected) to the forward (input) propagating wave:

$$r'(\hat{x},\lambda) + i4\pi r(\hat{x},\lambda) = -\frac{1}{2}\left[1 - r(\hat{x},\lambda)^2\right]\ln\left[n(\hat{x},\lambda)\right]' \tag{1}$$

where $\hat{x}$ is a normalized position coordinate denoting the proportion of the optical path length that has been traversed, L is the total optical path length of the modulated region, λ is the free-space wavelength of the light and " ′" refers to differentiation with respect to $\hat{x}$. Solving for r at 0 amounts to finding the complex reflection coefficient of a region of interest with a known refractive index profile. Equation (1) is of the form of a Ricatti equation, a class of nonlinear-first-order differential equations with no general analytical solution [13]. However, in the low reflection limit the nonlinear term - r^2 - can be neglected and Eq. (1) has a simple solution of Fourier transform form [12].

In this work, we extend our work to the on-chip optical waveguide platform, where the modulation of the refractive index can be represented by a modulation of the effective index of the waveguide mode through variation in the width of the silicon waveguide [W(x), Fig. 1(a)], as shown in Eq. (2):

$$r(\lambda) = \frac{1}{2}J(\lambda)\int_0^l \frac{dW}{dx}\exp\left[i2\pi\frac{2n_{eff}(\lambda)}{\lambda}x\right]dx \tag{2}$$

#214559 - $15.00 USD Received 23 Jun 2014; revised 26 Aug 2014; accepted 26 Aug 2014; published 9 Sep 2014

where x is the real position coordinate (in contrast to the previously used normalized position coordinate) along the waveguide axis, and $J(\lambda) = -\frac{1}{n_{eff}}\frac{dn_{eff}}{dW}$ takes into account the geometrical and material dispersion of the optical waveguide. As discussed earlier, we have dropped the positional dependence of r to indicate that we are finding the reflection coefficient of the whole modulated region. The dispersion (J) is calculated through an eigenfrequency analysis of the waveguide's cross-section (Lumerical MODE solutions). The integration in Eq. (2) is performed over the length of the width-modulated region of the waveguide (l). Note that Eq. (2) is of the form of a Fourier transform. (The integration limits can be extended to infinity as the integrand evaluates to zero everywhere outside the width modulated region.) This gives us a powerful method for finding the width profile $W(x)$ that results in the desired target reflection spectrum $r(\lambda)$, as illustrated in Eq. (3): $W(x)$ can be found via inverse Fourier transform followed by an integration from a known starting position and width. As an illustration of this approach, Fig. 1(c) shows an example target spectrum profile, while Fig. 1(d) shows the corresponding $W(x)$. The SEM micrograph of the fabricated structure featuring this width-modulation profile, realized in the SOI platform, is shown in Fig. 1(a).

$$\frac{\mathrm{d}W(x)}{\mathrm{d}x} = \int_{-\infty}^{\infty} \frac{2r(\lambda)}{J(\lambda)} exp\left[-i2\pi\frac{2n_{eff}(\lambda)}{\lambda}x\right]\mathrm{d}\left\{\frac{2n_{eff}(\lambda)}{\lambda}\right\} \tag{3}$$

It is worth noting that other authors have arrived at the same Fourier transform design method by approaching the problem from the point of view of volume holography [14], and the application of coupled-mode theory to weakly coupled gratings [15–18]. However, these approaches were either constrained to the low reflection limit or the authors concentrated on tailoring the phase in a high reflection limit. In this work we show that this approach can be expanded to produce high reflectance filters with broad, highly variable spectral features as well as phases. The filters previously numerically demonstrated in [15] feature generally low reflectance values, although the author does note that an iterative approach could lead to designs where the low reflectance is not mandatory [15]. Here, we use a similar iterative approach, but also derive methods for achieving high reflectances without the need for iteration. We stress that the method laid out in this work is not based on coupled-mode theory or holography approximations but is analytically derived directly from Maxwell's equations.

In arriving at Eq. (2) we assumed small amplitudes of the reflection coefficient (weak reflection at every segment of the width-modulated waveguide) by neglecting r^2 term. This approximation, however, may not be valid in certain cases, including high index contrast SOI waveguides. Indeed, when the designs obtained using Eq. (2) are tested either numerically (FDTD) or experimentally, the target $r(\lambda)$ spectra are not exactly reproduced (Fig. 1(e)). In addition to large amplitude of the reflection coefficient, this discrepancy can also be attributed to another approximation that was made in our analysis: the usage of effective mode index (n_{eff}) as an approximation to impedance of a dielectric waveguide mode. Highly confined modes locate a significant portion of their fields outside of the core dielectric, resulting in a discontinuity of the electric field component perpendicular to the dielectric boundary (Fig. 1(b)). As a result, the wave impedance ($|E_{transverse}|/|H_{transverse}|$) is not a well-defined quantity across the entire mode cross-section. In our original model [12], based upon plane waves, it was possible to establish an exact correspondence between the refractive index and the wave impedance, allowing us to reduce the problem of finding the reflection to a one dimensional differential equation. However, in the present work on-chip optical waveguide filters are considered, and additional steps need to be taken to compensate for the absence of an exact representation for the wave impedance.

#214559 - $15.00 USD Received 23 Jun 2014; revised 26 Aug 2014; accepted 26 Aug 2014; published 9 Sep 2014

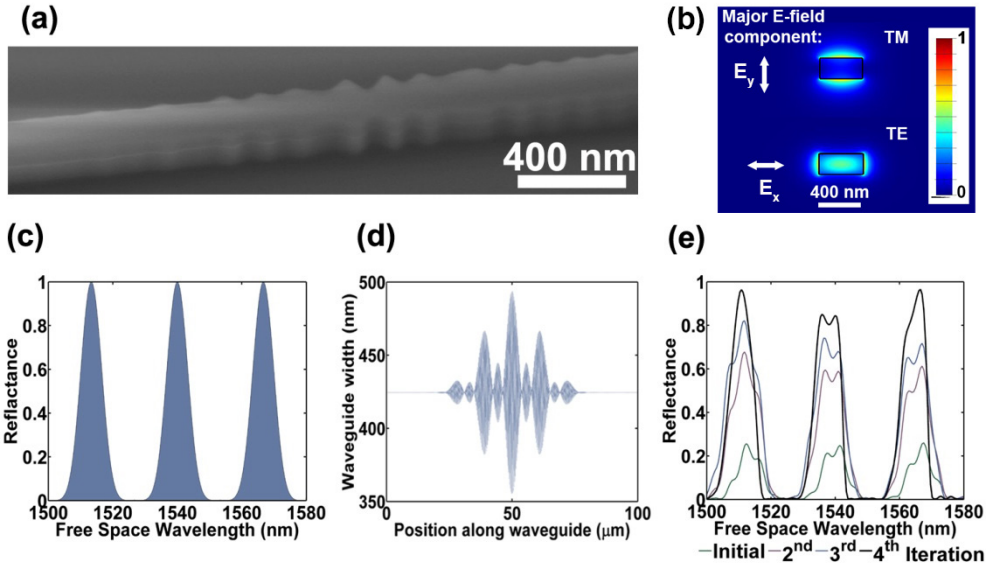

Fig. 1. (a) An SEM micrograph of a fabricated waveguide showing the $W(x)$ profile. (b) Cross-sections of the electric field intensity of the modes supported by our ridge waveguides. The TE-like mode features an E-field discontinuity at sides of the waveguide, while the TM mode's discontinuity is at the top and bottom of the waveguide. (c) An example target R(λ). (d) The width profile, W(x), that is obtained by applying the inverse Fourier transform obtained from Eq. (3) to the spectrum from b. (e) Simulated reflections, using FDTD analysis, from four iterations of our design method. The final step (thick black line) has come very close to replicating the spectrum from (b). Further optimizations are possible, though each subsequent iteration yields diminishing returns.

If we examine the cross-sections of the modes supported by our waveguides (Fig. 1(b)), we find that major E-field component of the TE-like mode (E_x) is not continuous along the direction of waveguide width (x-axis), while the major E-field component of TM-like mode (E_y) is. Therefore, the ratio $|E_{major}|/|H_{major}|$ is well-defined along the waveguide width (all H-field components are continuous in the absence of magnetic materials) in the case of TM-like modes. For this reason, one can expect that in the case of width-modulated waveguides (side-etched grating) considered here, TM-like modes follow our theoretical model much better than the TE-like ones. This can be attributed to the lack of E-field discontinuity at the location of the width modulation. Therefore, in the rest of the text we consider TM-like modes – unless otherwise noted. We mention, however, that in the case of thickness-modulated waveguide (grating etched into the waveguide top) TE modes follow our model better (data not shown), again due to the lack of field discontinuity at the location of the grating

After mitigating the effective index problem we considered two approaches to improve design performance and achieve a better correspondence between our intended and implemented reflection spectra – a job that becomes increasingly difficult at reflections approaching unity. The first is to use the linear properties of the Fourier transform to iterate the design process. This can be accomplished at relatively low computational cost thanks to modern waveguide simulation packages (MODE Solutions by Lumerical). We found that within 4 or 5 iterations we were able to get very near to an intended spectrum with large reflectance values.

Figure 2(a) illustrates the iterative design process that allows the design of filters with reflectance values that match the intended spectrum. $A(\lambda)$ is an artifact of this design process that compensates for the discrepancies arising from our assumption that $r^2 \to 0$ (it will also

#214559 - $15.00 USD Received 23 Jun 2014; revised 26 Aug 2014; accepted 26 Aug 2014; published 9 Sep 2014

deal with the effective index problem to some extent). Figure 1(e) shows simulated spectra of the iterative design process (in the case of TE-like modes) as A is recalculated and fed back into our design process.

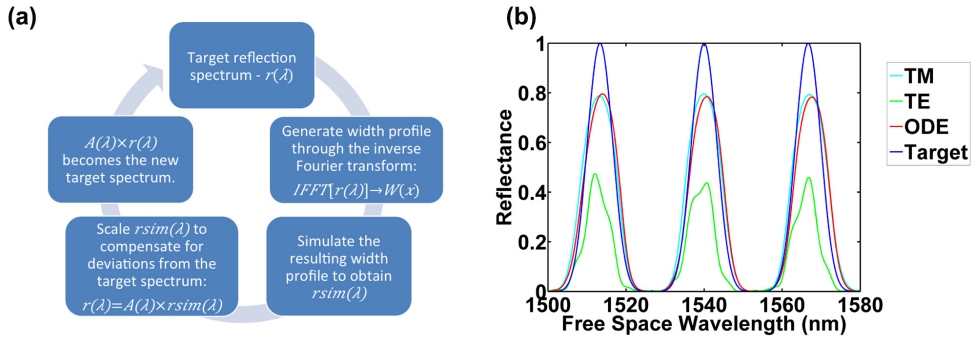

Fig. 2. (a) Iterative design process to compensate for inaccuracies due to assumptions in solution to Eq. (1). The result of the design process is checked via simulation, and any discrepancies in the resulting spectrum are used to feed back a wavelength dependent correction factor into the design process. (b) A comparison of the efficacy of our design method. The target reflection spectrum, shown in blue, was used to calculate the width profile using the Eq. (6). The reflection spectrum resulting from the obtained width profile was then found by solving Eq. (1) numerically, using an ordinary differential equation (ODE) solver, and results are plotted in red. The reflection spectra are also calculated using 3D FDTD modeling in the case of both TE and TM modes. Excellent agreement between ODE and FDTD solutions is found for TM mode, and is attributed to the lack of E-field discontinuity in the direction of interest (along waveguide width).

A second method is even more efficient, and is based on finding a better approximate solution to Eq. (1) than that obtained by neglecting the non-linear term. This can be accomplished by dividing both sides of the equation by $(1-r^2)$, and by grouping the terms on the left hand side of the equation into approximations of transcendental functions:

$$\frac{r(\hat{x},\lambda)'}{\left[1-r(\hat{x},\lambda)^2\right]}+i4\pi\frac{L}{\lambda}\frac{r(\hat{x},\lambda)}{\left[1-r(\hat{x},\lambda)^2\right]}=-\frac{1}{2}\ln\left[n(\hat{x},\lambda)\right]' \tag{4}$$

The first term on the left is identically the differential of $\tanh^{-1}(r)$ with respect to r, whereas the second term is only a very good approximation of $\tanh^{-1}(r)$. This allows us to rewrite Eq. (4) as:

$$\tan h^{-1}\left[r(\hat{x},\lambda)\right]'+i4\pi\frac{L}{\lambda}\tan h^{-1}\left[r(\hat{x},\lambda)\right]=-\frac{1}{2}\ln\left[n(\hat{x},\lambda)\right]' \tag{5}$$

The form of this equation allows us to instantly solve it, as it is identical to the previous version, up to a change of variable: r is replaced with the hyperbolic-arctangent of r. The power of this design method is illustrated in Fig. 2(b): one iteration produces results almost identical to the intended design. However, if better results are needed, due to the nonlinear nature of the hyperbolic function, non-linear optimization techniques need to be used. The operational equation used for determining the width profile of the waveguide to achieve a given reflectance spectrum becomes:

$$W(x)=\int_0^x dx\int_{-\infty}^{\infty}d\left\{\frac{2n_{eff}(\lambda)}{\lambda}\right\}\frac{2\tan h^{-1}\left[r(\lambda)\right]}{J(\lambda)}exp\left[-i2\pi\frac{2n_{eff}(\lambda)}{\lambda}x\right] \tag{6}$$

Finally, we note that in all simulations and experiments that follow, we have designed our filters with a linear phase response. While in most cases a linear phase response, exhibiting

#214559 - $15.00 USD Received 23 Jun 2014; revised 26 Aug 2014; accepted 26 Aug 2014; published 9 Sep 2014

zero group velocity dispersion, is preferable, there are situations – like certain kinds of pulse shaping and/or material dispersion compensation – where a non-linear phase response may be needed. We note that nonlinear phase response can be easily integrated into the design method obtained from Eq. (2). The use of similar filters has been demonstrated to counteract the dispersive elements of on-chip optics [16–18].

3. Ultra-fast pulse shaping

An important application of our filters and of arbitrary filters in general, is in shaping ultra-fast pulses. Bulky apparatus is currently used for ultra-fast shaping, and it requires precision alignment [19,20]. Though integrated solutions have been demonstrated for the chirping of pules [18] - our approach based on the inverse design method allows us to generate arbitrary pulse shapes in both phase and amplitude in a compact and stable manner. The small footprint of the filters allows for a high-density integration of devices with different responses, thus enabling a single external pulse to generate many different pulse shapes in parallel. Ultra-fast pulse shaping is of particular interest in quantum coherence control and other quantum optics experiments where a wider range of pulse shapes beyond "transform limited" is required [21,22].

The key to pulse shaping is the control of amplitude and phase over a wide wavelength range [23]. As Eq. (2) solves for r (the reflection coefficient) rather than R (the reflectivity, or $|r|^2$), the necessary conditions for ultra-fast pulse shaping are met. In this work we did not implement a non-linear phase because the pulses we were examining were not strongly affected by dispersion in the silicon waveguides.

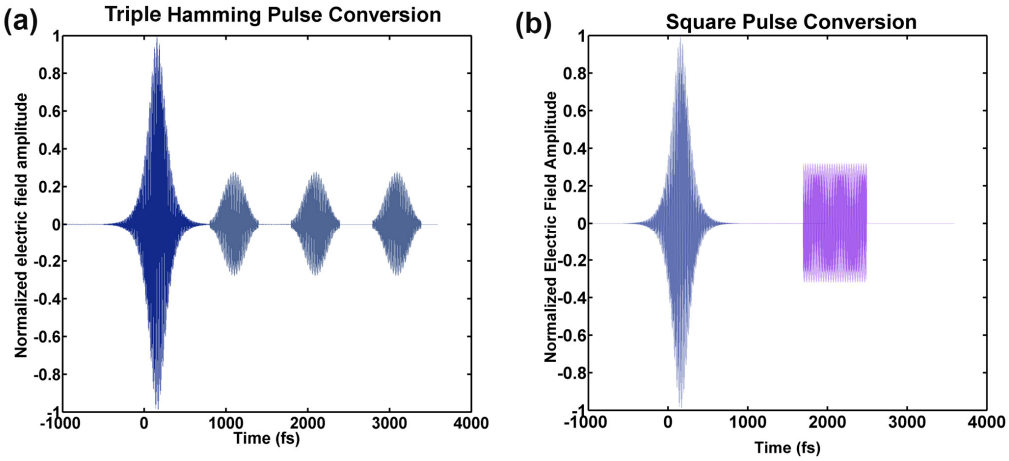

Fig. 3. Numerical analysis, using full 3D FDTD simulation, of ultra-fast pulse shaping. The $sech^2$ input pulse is incident on two different width modulated filters designed to reflect (a) "triple Hamming" pulse (shown in light blue), and (b) "square" pulse (shown in purple) with constant amplitude over a wide range. In both cases input $sech^2$ pulse is shown to the left of reflected pulses.

To illustrate the concept theoretically we designed two structures that turn a realistic 150 fs wide $sech^2$ pulse at 1550 nm center wavelength (e.g. coming out of an optical parametric oscillator) into: i) triple pulses with a Hamming [24] envelope, and ii) a square-envelope pulse with a constant amplitude over a wide region. In both cases, the on-chip filter is designed using our inverse-design principle based on Eq. (6) as discussed above. The filters were designed for the TM mode of 220 nm thick SOI clad in SiO_2. The spectral shapes of the filters can be seen in Figs. 4(b) and 4(c). To validate our results, we used 3-D finite difference time domain (FDTD, Lumerical Inc.) simulations to model the response of designed filters. Indeed, Figs. 3(a) and 3(b) show that a single $Sech^2$ pulse launched into two different width-modulated SOI waveguides, can be converted into three distinct Hamming pulses and a square pulse, respectively. All simulations are three dimensional with the mesh grid size of 1

#214559 - $15.00 USD Received 23 Jun 2014; revised 26 Aug 2014; accepted 26 Aug 2014; published 9 Sep 2014

nm, which is similar to the e-beam lithography resolution available to us. This is an excellent first demonstration for the viability of integrated femtosecond pulse shaping.

The limitation of this shaping method is that it is entirely based on the reflection of the input light, so the available output pulses have a spectrum limited by the spectrum of the input light. The magnitude of the power reflected will also be less than or equal to that of the input pulse. This results in smaller amplitudes in the reflected signal as can be seen in Figs. 3(a) and 3(b). The only way to avoid losing power is to use the filters that alter the phase of the pulse while leaving the amplitude untouched. Within these restrictions our filters behave admirably, giving high visibility peaks and the expected envelope shapes.

4. Fabrication and testing

When transferring a continuous modulation of a waveguide width onto an SOI sample through e-beam lithography, two problems occur. The first, is related to the finite length of devices that can be fabricated using e-beam lithography: the finite length of the device determines the highest bandwidth of the reflection spectrum that can be represented appropriately if an r spectrum with large 'tails' in its Fourier transform is chosen, there will be significant degradation in the resulting spectrum because a large proportion of the Fourier components will be lost. Second, errors arise from the finite resolution of e-beam lithography washing out the fine features in the r spectrum. Viewed through the prism of classical digital signal processing, these two issues would be equivalent to not sampling the data for a sufficiently long period in the time domain, and to obtaining an analog to digital conversion with insufficient bits to properly resolve the amplitude of the signal. This allows us to choose a "sweet spot" of the filter bandwidth and the length of the filter so that the $W(x)$ profile can be defined using the electron-beam (e-beam) lithography tool available to us.

For experimental demonstration, we fabricated the width modulated filters on SOI wafers (SOITEC) with a 220 nm device layer and a 2 μm buried oxide layer. The waveguides were written using a negative resist (XR 1541-6%) and 100 kV electron-beam lithography (Elionix 7000). The exposure window was a 300 μm square with a dot-pitch of 1.25 nm. After development (TMAH 2.5%) the pattern was transferred to the device layer using reactive-ion etching (C_4F_8 and SF_6). SU-8 Polymer waveguides were defined using e-beam lithography for spot size conversion. Finally, the device was capped using PE-CVD deposited silicon dioxide to enable facet polishing. Figure 4(a) shows an SEM micrograph of an example device prior to PE-CVD deposition.

Filter characterization was performed with a scanned tunable laser (Santec TLS-510 C-Band). Light was coupled onto the chip's TM mode through a tapered, lensed fiber (Oz optics). An on-chip, 3-dB directional coupler was used to extract the reflected signal to an output arm and back to an SU-8 waveguide as depicted in Fig. 4(a). Figures 4(b) and 4(c) show example target spectra alongside experimentally measured spectra; the agreement between the two is excellent. In the absence of the equipment required to measure a time domain response of our filters, and based on the excellent agreement of the spectral response obtained by theory, 3D FTDT simulations and experimental characterization, we conclude that these filters would perform to their designed specification in terms of shaping pulses.

#214559 - $15.00 USD Received 23 Jun 2014; revised 26 Aug 2014; accepted 26 Aug 2014; published 9 Sep 2014

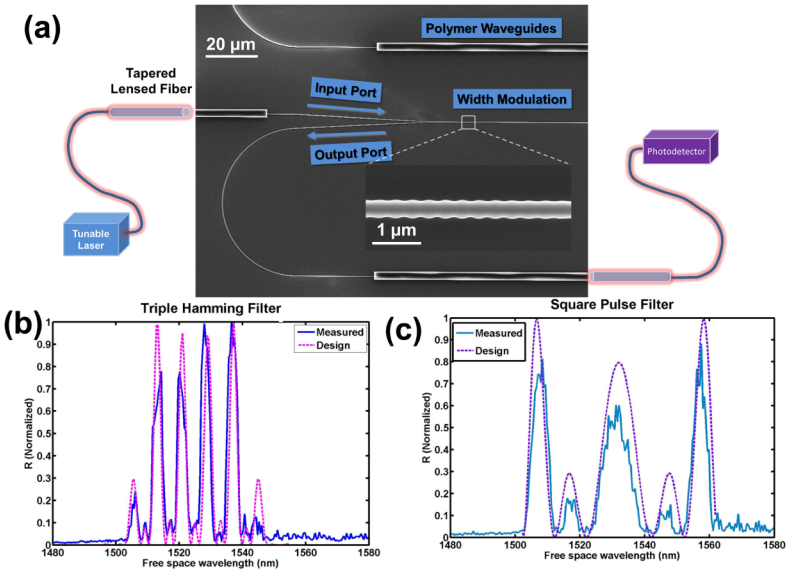

Fig. 4. (a) SEM micrograph of example device; the inset shows a magnification of the width modulated region. Cartoons show the flow of the experiment: light is launched from a tunable telecom laser through a lensed fiber, is then coupled through a polymer waveguide to the silicon waveguides through an inverse taper. The light reflected from the modulated waveguides is extracted using a directional coupler to another polymer waveguide, and finally collected through a second lensed fiber into a photodetector. The light on-chip is propagating in the TM mode (b) The spectral shape of the "triple Hamming" filter, overlayed with the target design (c) The spectral shape of the square-pulse filter as probed by the tunable laser. The dashed overlay represents our target design. The measured spectra in both (b) and (c) are normalized by the magnitude of the light transmitted through the filter. We note that in both cases the signal is distorted by Fabry-Perot resonances in the system (e.g. from the SU-8 waveguide facets) as well as truncation effects due to the finite size and resolution of the width-modulated filters.

5. Conclusions and future work

We have demonstrated a reverse method for designing arbitrary filters with the footprint of an on-chip waveguide. We fabricated and measured filters designed using this method, and they exhibited excellent agreement with our theoretical prediction. In addition to allowing the design of arbitrary phase and amplitude filters these structures show a great promise in shaping ultrafast pulses as demonstrated through FDTD simulations. Therefore, we believe that this approach provides a novel and feasible platform for control of ultra-fast pulses with greatly reduced footprints and experimental complexity. In the future, we will look to implementing ultra-fast pulse shaping as well as using dynamic methods to tune the filter response.

Acknowledgments

The authors would like to thank K. Shtyrkova and E. Ippen for their advice on ultra-fast pulses. This work was performed in part at the Center for Nanoscale Systems (CNS), a member of the National Nanotechnology Infrastructure Network (NNIN), which is supported by the National Science Foundation under NSF award no. ECS-0335765. CNS is part of Harvard University. This work was supported in part by the Air Force Office of Scientific Research Award # FA9550-09-1-0669-DOD35CAP. The manuscript was written with the contributions of all authors. Theoretical work and design was done by Y.Z. Device fabrication and experimental characterization was carried out by I.W.F. All authors have approved the final version of the manuscript.